Chemical Engineering Journal 169 (2011) 371–378

Contents lists available at ScienceDirect

Chemical Engineering Journal

journal homepage: www.elsevier.com/locate/cej

Antireflection/antifogging coatings based on nanoporous films derived from layered double hydroxide

Jingbin Han, Yibo Dou, Min Wei*, David G. Evans, Xue Duan

State Key Laboratory of Chemical Resource Engineering, Beijing University of Chemical Technology, Beijing 100029, PR China

ARTICLE INFO

Article history:
Received 25 November 2010
Received in revised form 20 February 2011
Accepted 25 February 2011

Keywords:
Layered double hydroxides
Antireflection
Antifogging
Layer-by-layer
Coatings

ABSTRACT

Multifunctional mixed metal oxide (MMO) thin films on quartz substrates have been fabricated by layer-by-layer assembly of layered double hydroxide (LDH) nanoparticles and poly(sodium styrene 4-sulfonate) (PSS) followed by calcination, which exhibited properties of both antireflection (AR) and antifogging (AF). The AR and AF performances are related to the low refractive index and superhydrophilicity originating from the nanoporous structure. The influences of deposition cycle, LDH particle size and calcination temperature on AR and AF behavior were thoroughly studied. A maximum transmittance of 98.7% at 650 nm and a minimum time of 0.2 s for a droplet to spread flat (water contact angle ~0°) were achieved with LDH particle size of 110 nm, 10 cycles of deposition and calcination temperature of 450 °C. Therefore, this work provides a facile approach for the fabrication of multifunctional coatings, which can be potentially used in photovoltaic devices, optical lens and underwater imaging systems.

1. Introduction

Antireflective (AR) coatings have recently attracted much interest for their applications in photovoltaic, displaying devices and all kinds of optical lenses [1–3], owing to their ability to enhance the transmittance of light and remove ghost images. The principle of AR coatings is based on the destructive interference of reflected light from air-film and film-substrate interfaces. An ideal homogeneous single-layer AR coating satisfies the following conditions [4]: (1) the thickness of the coating is $\lambda/4$, where λ is the wavelength of the incident light; (2) $n_c = (n_a n_s)^{1/2}$, where n_c, n_a and n_s are the refractive indices of the coating, air and substrate, respectively. For a glass substrate ($n_s = \sim 1.5$), the refractive index of AR material should be ~1.22. However, nature materials with such low refractive index are either rare or expensive to obtain in thin film form. As a substitute, nanoporous materials are usually chosen as AR coatings, since the introduction of the nanopores can reduce the refractive index of the coatings and satisfy the AR requirement [5–7]. The refractive index of porous coatings can be well tailored by controlling the percentage of pores introduced, in which larger percentage of pores leads to lower refractive index. Up to now, many methods have been developed to obtain nanoporous film materials for use as AR coatings, including sol–gel process [8], phase-separation [9], sacrificial porogen approach [10–12], layer-by-layer (LBL) deposition of nanoparticle multilayers [13,14], plasma-enhanced chemical vapor deposition [15] and deposition of nanorods or nanowires [16,17]. Compared with other methods, the LBL assembly technique holds a great potential in the fabrication of AR coatings because of its simplicity in preparation of films with large area and its facility in depositing films on non-flat surfaces [18,19].

Although the materials and methods for the preparation of porous AR coatings are diverse, there are still several serious issues should be concerned for the application of the resultant AR coatings, especially the influence of water vapor existing in the external environment. Water vapor molecules condense and form water droplets on the surface, resulting in scattering and reflection of light, which in turn decreases the transmittance of the AR coating. A superhydrophilic coating, on which the water contact angle is less than 5° within 0.5 s as soon as a water droplet contacts such surface, can solve this problem [20–22]. Superhydrophilic coatings can significantly suppress the fogging behavior by the rapid spread and flow of water droplets on their surface and therefore eliminate the light scattering caused by water droplets. In fact, AR coatings combined with an antifogging (AF) capability are highly desired in daily used eyeglasses, swimming goggles, periscopes, lenses in endoscopic surgery, and so forth.

Layered double hydroxides (LDH) are layered anionic clays generally expressed by the formula $[M^{2+}_{1-x}M^{3+}_{x}(OH)_2](A^{n-}) \cdot mH_2O$, where M^{2+} and M^{3+} are di- and trivalent metal cations and A^{n-} is a counter anion [23–26]. The host structure consists of brucite-like layers of edge-sharing $M(OH)_6$ octahedra, and the partial substitution of M^{3+} for M^{2+} results in positively-charged host layers, balanced by the interlayer anions [27–30]. It is well-known that calcination of LDH at intermediate temperatures in the range

* Corresponding author. Fax: +86 10 64425385.
E-mail addresses: weimin@mail.buct.edu.cn, weimin-hewei@163.com (M. Wei).

1385-8947/$ – see front matter © 2011 Elsevier B.V. All rights reserved.
doi:10.1016/j.cej.2011.02.070

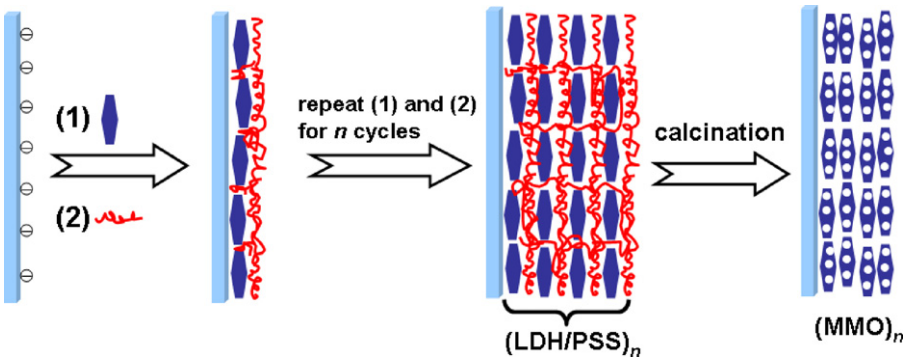

Scheme 1. Schematic illustration for the fabrication of MMO nanoporous coatings.

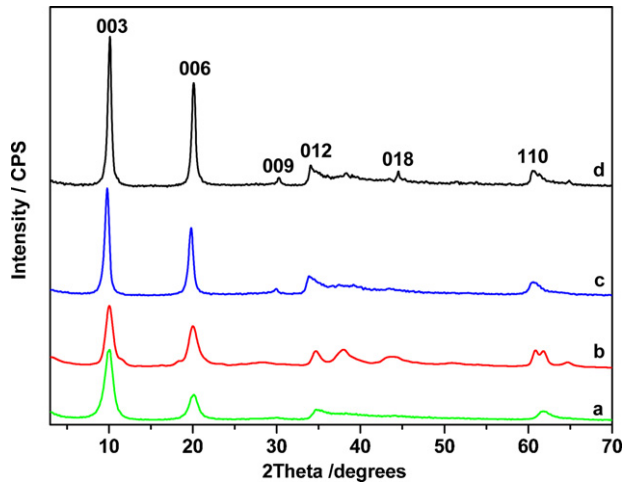

Fig. 1. XRD patterns for the MgAl-LDH materials prepared at 110 °C with different aging time: (a) 4 h, (b) 8 h, (c) 18 h and (d) 48 h.

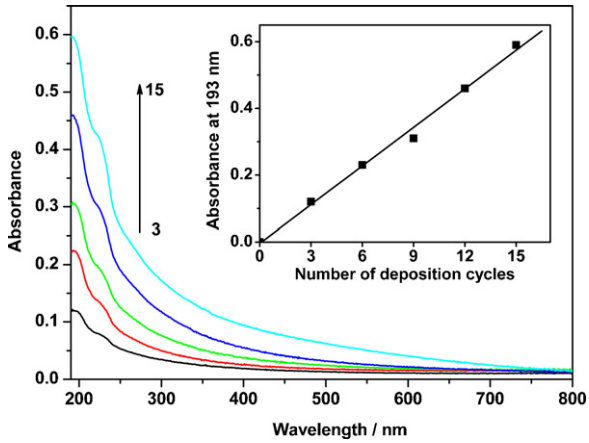

Fig. 3. UV–vis absorption spectra of the (LDH-25/PSS)$_n$ (n = 3–15) films assembled on quartz glass substrates. The absorbance at 193 nm is plotted against the bilayer number in the inset.

300–600 °C leads to the formation of mixed metal oxides (MMO) which possess porous structures and large specific surface areas as well as good thermal stability [31–33]. In our previous work [34], a nanoporous MMO coating was fabricated by calcination of (LDH/PSS)$_n$ ('n' denotes the number of deposition cycles) multilayer films on quartz glass substrate, which exhibited erasable AR properties with excellent mechanical stability and good adhesion to substrates. However, detailed AR properties of the MMO coating

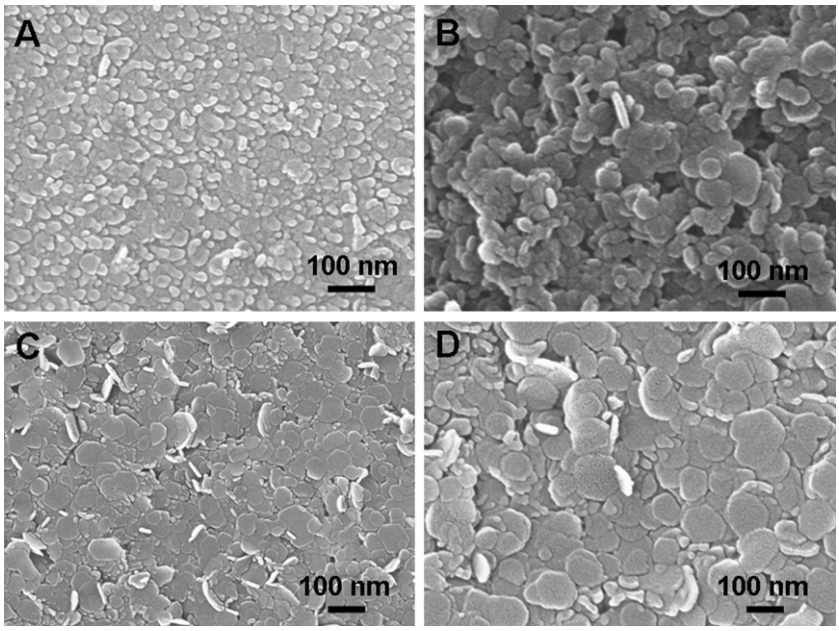

Fig. 2. SEM images for the MgAl-LDH materials prepared at 110 °C with different aging time: (a) 4 h, (b) 8 h, (c) 18 h and (d) 48 h.

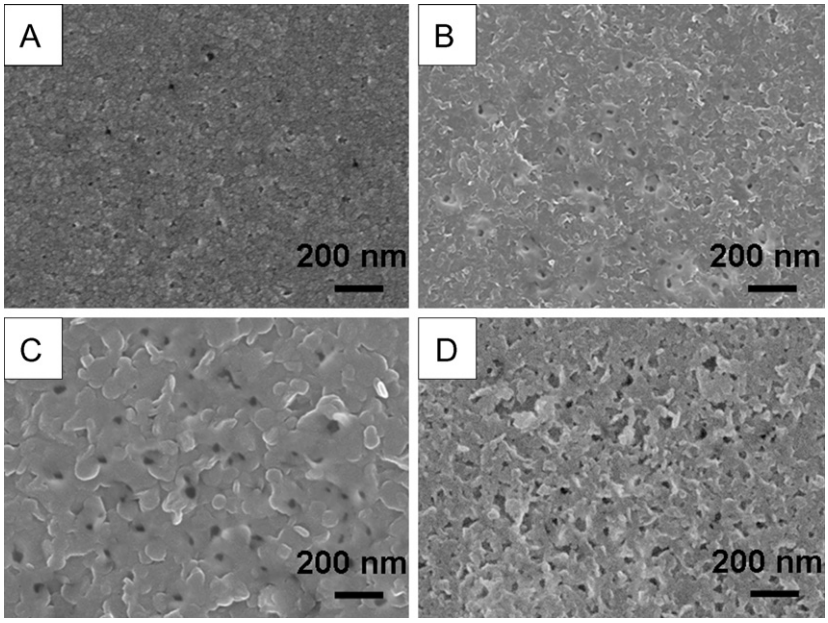

Fig. 4. SEM images of (A) $(MMO\text{-}25)_{10}$, (B) $(MMO\text{-}45)_{10}$, (C) $(MMO\text{-}70)_{10}$ and (D) $(MMO\text{-}110)_{10}$ films deposited on quartz substrates (reproduced from our previous work Ref. [34]).

dependent on the fabrication parameters (e.g. particle size, number of deposition cycle, calcination temperature) as well as its applicability in practical environment remain unresolved.

In this work, nanoporous MMO films were fabricated *via* LBL assembly of $(LDH/PSS)_n$ films followed by calcination. The presence of nanopores in MMO coatings leads to multi-functionalities including both AR and AF properties, which are dependent on the number of deposition cycle, size of LDH nanoparticles and calcination temperature. The transmittance of the substrate increases to a maximum and then decreases along with the increase of coating thickness, owing to the diffuse scattering induced by the increased surface roughness. Larger nanoparticles of LDH precursor are more effective in enhancing transmittance and hydrophilicity than smaller nanoparticles. Systematic investigation gave an optimal condition for the fabrication of MMO film with excellent AR and AF behavior: a maximum transmittance of 98.7% at 650 nm and a minimum spread time of 0.2 s for a droplet (water contact angle ~0°) were achieved by calcination of the $(LDH/PSS)_{10}$ film with LDH particle size of 110 nm at 450 °C. Therefore, the present study provide a feasible strategy for the design and fabrication of antireflective and antifogging coatings, which can be used in optical devices and antifogging manipulation.

2. Experimental

2.1. Preparation of colloidal LDH suspension

Colloidal LDH suspension was prepared according to the reported procedure [35]. Typically, 100 ml of solution A ($Mg(NO_3)_2{\cdot}6H_2O$: 0.2 M and $Al(NO_3)_3{\cdot}9H_2O$: 0.1 M) and 400 ml of solution B (NaOH: 0.15 M) were simultaneously added to a colloid mill with rotor speed of 3000 rpm and mixed for 1 min. The result-

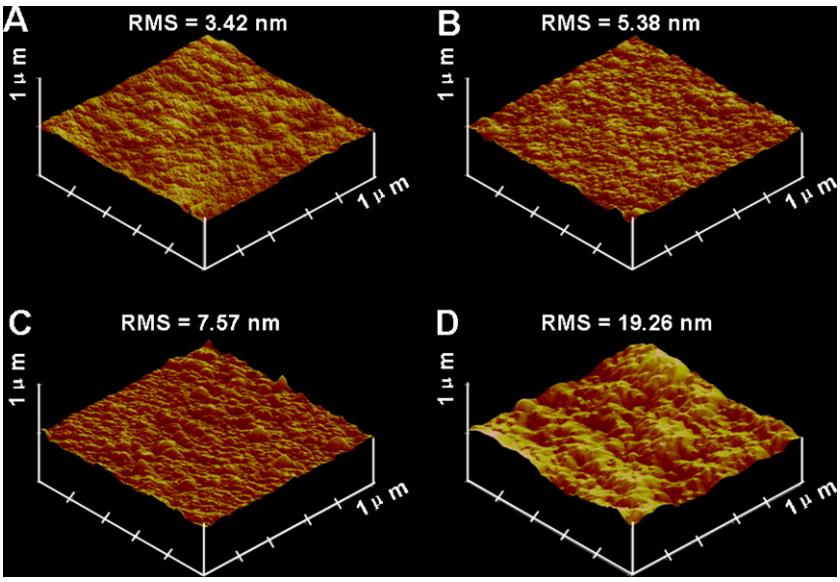

Fig. 5. AFM images of the $(MMO\text{-}25)_n$ films deposited on silicon wafer substrates: (A) $n = 8$, (B) $n = 16$, (C) $n = 24$ and (D) $n = 30$.

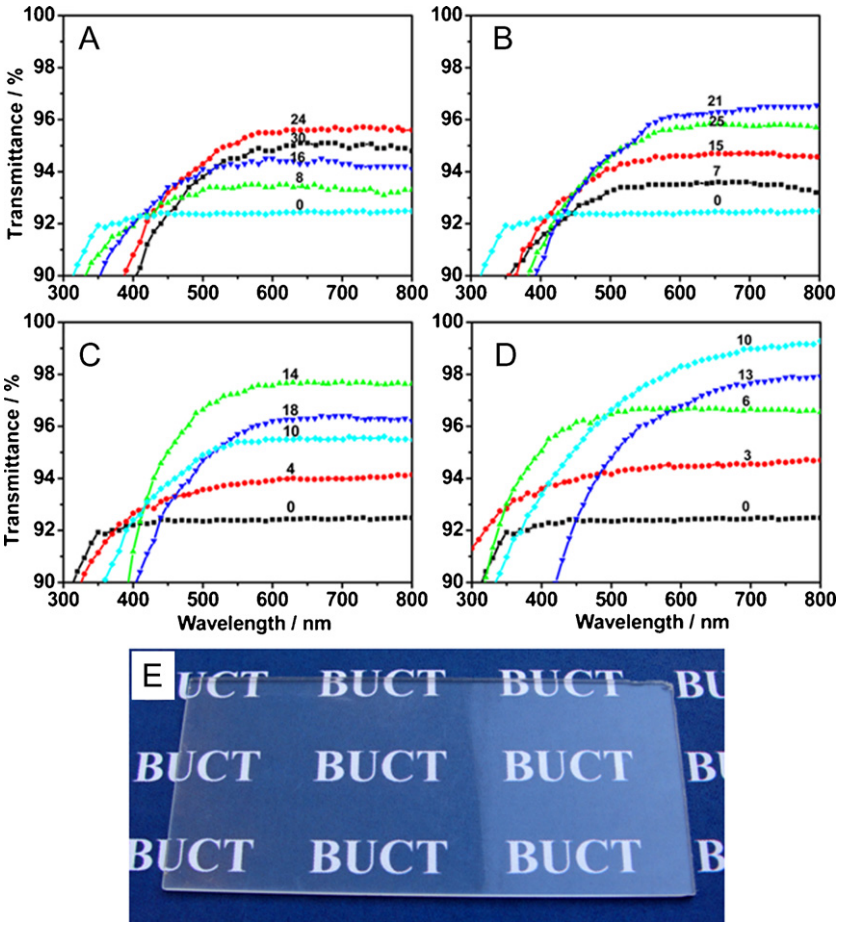

Fig. 6. Transmission spectra of (A) $(MMO\text{-}25)_n$, (B) $(MMO\text{-}45)_n$, (C) $(MMO\text{-}70)_n$, (D) $(MMO\text{-}110)_n$ films deposited on quartz substrates with different bilayer number; (E) Photograph of a quartz substrate exposed to sunlight. The left portion was coated with $(MMO\text{-}110)_{10}$ film and the right portion was bare quartz (reproduced from our previous work Ref. [34]).

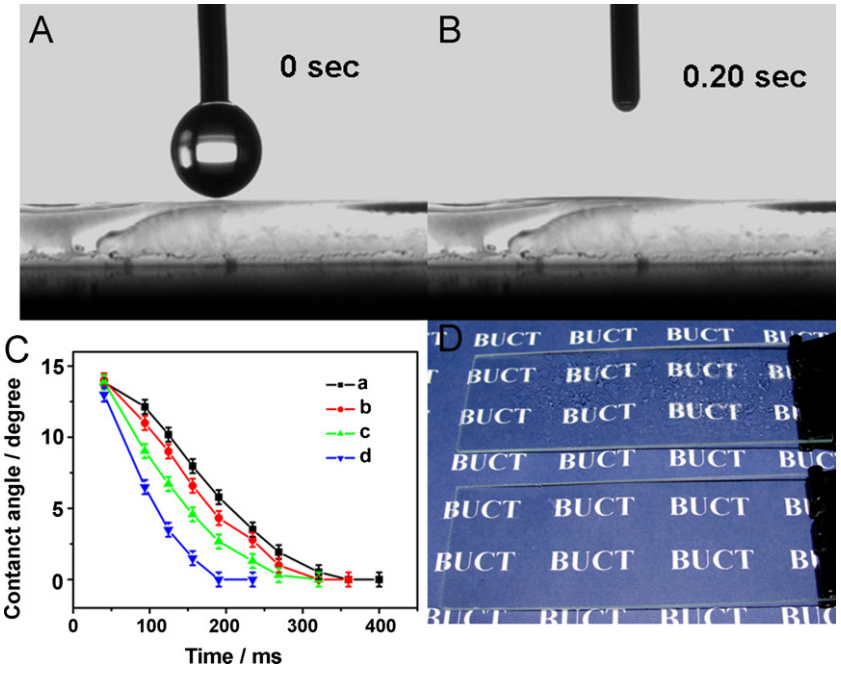

Fig. 7. (A) and (B) Still images from video contact angle measurements for a water droplet (2 μL) spreading on a quartz substrate coated with $(MMO\text{-}110)_{10}$ film; (C) Time-dependent changes in instant contact angle for various coatings: (a) $(MMO\text{-}25)_{24}$, (b) $(MMO\text{-}45)_{21}$, (c) $(MMO\text{-}70)_{14}$ and (d) $(MMO\text{-}110)_{10}$; (D) Photograph of a quartz substrate coated with $(MMO\text{-}110)_{10}$ film on both sides (bottom) and a bare quartz substrate (upper) taken from a refrigerator (about −12 °C) to the humid laboratory air (relative humidity ≈45%).

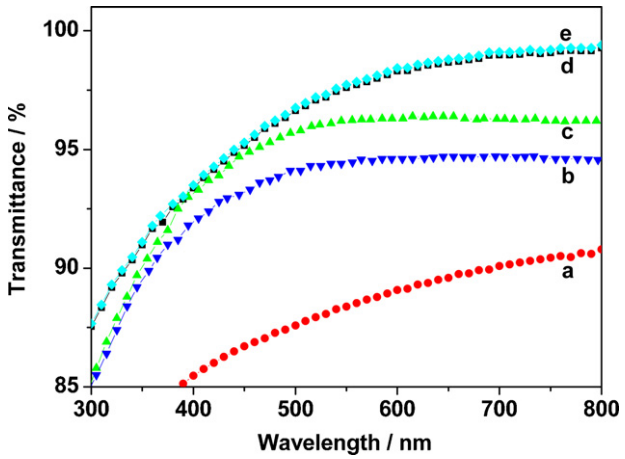

Fig. 8. Transmission spectra of (a) the as-prepared (LDH-110/PSS)$_{10}$ film and the resulting coatings after calcination at (b) 200 °C, (c) 350 °C, (d) 450 °C and (e) 500 °C deposited on quartz glass substrate.

ing LDH slurry was obtained *via* centrifugation and washed twice with deionized water and then dispersed in 400 mL of deionized water. This aqueous suspension was transferred into a stainless steel autoclave with a Teflon lining. After hydrothermal treatment at 110 °C for a period of time (4–48 h), stable homogeneous LDH suspension with various particle size was obtained.

2.2. Construction of antireflection and antifogging coatings

Multilayer films of LDH nanoparticles/PSS were fabricated by electrostatic layer-by-layer (LBL) method. Quartz glass slide or silicon wafer were pretreated in a bath of methanol/HCl (1/1, v/v) and then concentrated H_2SO_4 for 30 min each to make the substrates surface hydrophilic and negatively charged. The overall LBL process consists of a cyclic repetition of the following steps: (a) dipping the pretreated substrates into the colloidal LDH suspension containing MgAl-LDH nanoparticles for 10 min, followed by rinsing with deionized water thoroughly; (b) dipping into an aqueous solution of PSS (1.0 g/L) for 10 min and washed with deionized water. Subsequently, a series of these operations for LDH nanoparticles and PSS were repeated n times to obtain multilayer films of (LDH/PSS)$_n$. The resulting films were finally rinsed with deionized water and dried at ambient temperature. The substrates coated with (LDH/PSS)$_n$ film were annealed at appropriate temperature for 3 h to remove the porogen species and produce a mixed metal oxide (MMO) film with nanoporous structure. The typical procedures for the fabrication of AR and AF multifunctional coatings are shown in Scheme 1.

2.3. Sample characterization

Powder X-ray diffraction (XRD) patterns of the samples were collected using a Shimadzu XRD-6000 diffractometer under the following conditions: 40 kV, 30 mA, graphite filtered Cu Kα radiation (λ = 0.1542 nm). Scanning electron microscopy (SEM) images were obtained on a Zeiss Supra 55 field emission scanning electron microscope. Atomic force microscopy (AFM) images were collected using a NanoScope IIIa AFM from Veeco Instruments in the tapping-mode in air. UV–vis absorption and transmittances spectra were recorded using a Shimadzu UV-2501PC spectrometer. Static water contact angles were measured using a sessile drop at three different points of each film sample using a commercial drop shape analysis system (DSA100, KRüSS GmbH, Germany) at ambient temperature. The volume of water droplets used for measurement is 2 μL.

3. Results and discussion

3.1. Preparation of LDH colloidal suspension and assembly of multilayer coatings

The X-ray diffraction patterns of MgAl-LDH materials exhibit the typical layered features with a high crystallinity, as shown in Fig. 1. In each case, the XRD pattern displays the characteristic reflections of the LDH structure with a series of (0 0 l) peaks appearing as narrow, symmetric, strong lines at low angle. The basal spacing of all the LDH samples is ~0.873 nm and the lattice parameter a is 0.305 nm, close to the reported value for nitrate-containing LDH phase [36–39]. The well-dispersed LDH suspension was transparent and stable without any precipitation when stored in an N_2 atmosphere for more than one month. The morphology of LDH nanoparticles was examined by SEM (Fig. 2), which reveals that the individual MgAl–NO_3 LDH nanoparticles with narrow size distribution were obtained after hydrothermal treatment. The particle size can be steadily controlled by changing the hydrothermal time. LDH colloidal suspension with average particle size of 25 nm (denoted as LDH-25), 45 nm (LDH-45), 70 nm (LDH-70) and 110 nm (LDH-110) were obtained with treatment time of 4, 8, 18 and 48 h, respectively.

It was reported the colloidal LDH nanoparticle suspension in aqueous solution shows a positive zeta potential in the range 30–50 mV [40], indicating that the external surface of LDH nanoparticles is positively charged. Therefore, colloidal LDH nanopaticles can be used as building blocks without any surface modification for the assembly of functional multilayer films with negatively charged electrolytes by the electrostatic LBL technique. In this work, the positively charged LDH nanoparticles were alternately deposited with negatively charged PSS to fabricate LDH/PSS multilayer films. The subsequent growth of LDH/PSS multilayer film was monitored by means of the UV-vis absorption bands of PSS (193 and 225 nm) as depicted in Fig. 3. From the inset of Fig. 3, a linear increase in absorbance at 193 nm upon increasing the bilayer number was observed, indicating a stepwise and regular growth of LDH nanoparticle/PSS multilayer films.

The LDH/PSS multilayer films deposited on quartz substrates were calcinated in an oven at 450 °C for 3 h to remove the organic components and interlayer anions of LDH, resulting in the formation of MMO films with a nanoporous structure. Fig. 4 shows the SEM images of (MMO-m)$_n$ coatings obtained by calcination of (LDH-m/PSS)$_n$ films (m denotes the particle size of LDH precursor; n represents the number of deposition cycle for the (LDH/PSS)$_n$ films). Dense and uniform nanopores can be clearly observed on the surface of (MMO-m)$_{10}$ coatings, and the pore size increased from 10 nm to 60 nm upon increasing the precursor LDH particle size. The atomic force microscope (AFM) images (Fig. 5) of the (MMO-25)$_n$ films with different bilayer number (n = 8, 16, 24, 30) further reveals the porous structure. Clearly aggregated nanoparticles create hill-to-valley surface cavities that typically extend about 20–60 nm in depth. The root-mean-square (RMS) roughness of the MMO film increases from 3.42 to 19.26 nm as the bilayer number varies from 8 to 30. The morphological feature of the film would be beneficial to enhance the transmittance of the substrates as well as superhydrophilicity, which will be discussed in the next section.

3.2. Multifunctionality of MMO coatings

The AR properties of the calcinated LDH/PSS films were investigated by using the transmittance measurement. Fig. 6A shows the transmission spectra of quartz substrates coated with (MMO-25)$_n$ (n = 8, 16, 24, 30) film. The transmission spectrum of a bare quartz substrate was also provided for comparison, which exhibits a transmittance of ~92.1% in the spectral range between 300 and 800 nm.

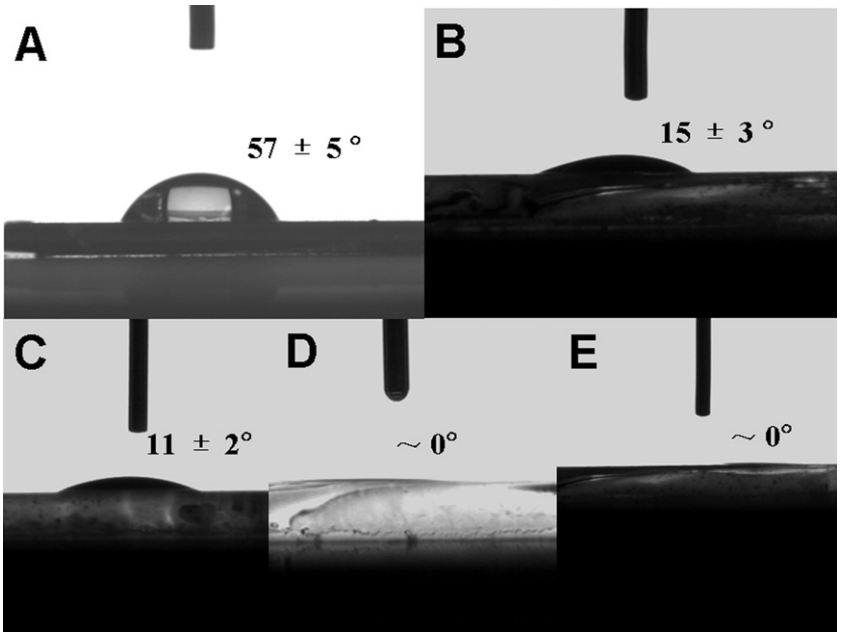

Fig. 9. Water contact angles of (A) the as-prepared $(LDH\text{-}110/PSS)_{10}$ film and the resulting coatings after calcination at (B) 200 °C, (C) 350 °C, (D) 450 °C and (E) 500 °C deposited on quartz glass substrates.

The transmittance of quartz substrates coated with $(MMO\text{-}25)_n$ films was dramatically enhanced compared with the bare substrate, indicating the AR property of the resultant coatings. Along with the increase of n, the transmittance first increased from $n = 8$ (~93.1%) to $n = 24$ (~95.9%) at the wavelength of 650 nm; however, it decreased with further increase of deposition cycle ($n = 30$: ~95.0%). The decrease in transmittance results from the enhanced diffuse scattering accompanying the increase of surface roughness, which has already been confirmed by AFM characterization. A similar trend was also observed for the $(MMO\text{-}45)_n$, $(MMO\text{-}70)_n$ and $(MMO\text{-}110)_n$ coatings; i.e., the transmittance reached a maximum value with a specific thickness and then decreased for thicker samples. The maximum transmittance values were found to be 95.9%, 96.7%, 97.7% and 98.7% for the films of $(MMO\text{-}25)_{24}$, $(MMO\text{-}45)_{21}$, $(MMO\text{-}70)_{14}$ and $(MMO\text{-}110)_{10}$, respectively (Fig. 6A–D). Therefore, the transmission of MMO films can be well tuned by changing the particle size of LDH precursor as well as the deposition cycle. The optimal AR property of the $(MMO\text{-}110)_{10}$ film was also exhibited straightforwardly in Fig. 6E. The clear words below the AR coating demonstrate the increased transparency and reduced reflection, whereas the bare substrate reflects the sunlight significantly, and the words below are not as clear as those of the AR coating.

Taking into account the potential application of these AR coatings in humid environment, the water wetting behavior of the MMO films was studied by water contact angle measurements with a water droplet of 2 μL as the indicator. As shown in Fig. 7A and B, as the water droplet contacted the surface coated with $(MMO\text{-}110)_{10}$ film, it spread over the surface completely within 0.2 s, demonstrating a superhydrophilic surface. The hydrophilic MMO material accompanied with the three dimensional porous structure further increased the hydrophilicity of the film because of the nanowicking of water into the network of capillaries present in the coating. The time-dependent changes in water-droplet contact angle of the coating with various precursor LDH particle size are shown in Fig. 7C, demonstrating excellent superhydrophilicity for all the samples. The time for water droplet spread flat ranges in 0.4–0.2 s as the LDH particle size varies from ~25 to ~110 nm. Superhydrophilic coatings can significantly suppress the fogging behavior, since condensed water droplets will spread flat almost instantaneously to form a thin sheet-like water membrane [20–22]. In this way, light scattering by the condensed water droplets is eliminated. The thin water membrane eventually disappears either by sliding down under the influence of gravity or by evaporation. The photograph in Fig. 7D illustrates the antifogging behavior of the superhydrophilic MMO coatings. A quartz substrate coated with the $(MMO\text{-}110)_{10}$ film on both sides and a bare quartz slide were cooled to about −12 °C in a refrigerator, and then were exposed to the humid air simultaneously (relative humidity ≈45%). As shown in the upper part of Fig. 7D, the bare quartz slide fogged immediately. The words below the slide were blurred by the strong light scattering resulting from the surface dewdrops. In sharp contrast, the quartz slide coated with the superhydrophilic MMO film remained highly transparent and the words below were clearly seen (bottom part of Fig. 7D).

3.3. Effects of calcination temperature on the AR and wetting behavior

The AR and AF properties of $(MMO)_n$ coatings originate from their nanoporous structure. Different calcination temperature induces diverse proportion of void fraction in the coating, which affects the final AR and AF behavior. The $(LDH\text{-}110/PSS)_{10}$ coating was treated at 200, 350, 450 and 500 °C for 3 h respectively, in order to study the influence of calcination temperature on the transmittance/wettability of the film. As shown in Fig. 8, transmittance of the film increases gradually from 87.4% to 98.7% at 650 nm as the calcination temperature increases from 200 to 450 °C. Furthermore, effects of calcination temperature on the hydrophilicity of resultant coatings were also investigated. The water contact angle of the LDH/PSS film (~57°, Fig. 9A) is much larger than that of the MMO coatings after calcination. It decreased from ~15° to ~0° as the calcination temperature increased from 200 to 450 °C. Further increase of the calcination temperature to 500 °C showed insignificant influence on the AR and hydrophilicity, indicating the achievement of decomposition equilibrium for the porogen (organic component and interlayer species of LDH) and the formation of stable nanopores at 450 °C.

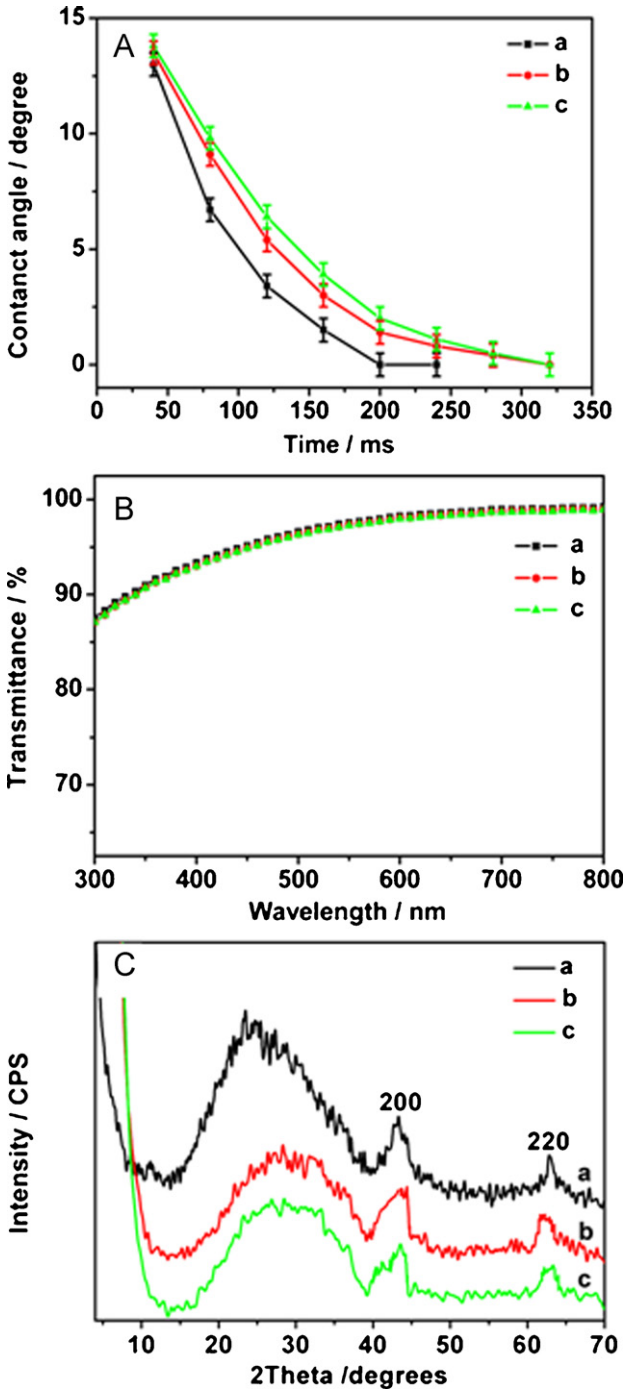

Fig. 10. (A) Changes in the contact angle of a water droplet as a function of time, (B) transmittance spectra and (C) XRD patterns for various samples: (a) the freshly prepared $(MMO\text{-}110)_{10}$ film and the same film after (b) 50 and (c) 100 days of storage under ambient conditions.

3.4. Long-term stability of the AR and AF coatings

In this work, the long-term stability of both AR and AF properties for the MMO films was investigated, which is extremely important for practical applications. The superhydrophilicity of the coating was maintained after 100 days storage (Fig. 10A). The spread time for the water droplet on the porous MMO coating increased slightly (from 0.2 s to 0.32 s), indicative of the stability for the AF property. Compared with TiO_2-based coatings [41–43] which lose their superhydrophilic properties with the absence of UV irradiation, MMO coatings in this work retained their superhydrophilicity even in the dark owing to the different mechanism of superhydrophilicity. As described above, the presence of nanopores in the MMO film structure leads to nanowicking of water into the network of capillaries in the coatings; therefore, the AF properties are retained without UV irradiation. Furthermore, the AR properties did not show any decrease after storage of the porous MMO films under ambient conditions for 100 days (Fig. 10B), demonstrating the excellent stability of the AR coatings. The highly durable stability of the porous MMO coatings was further confirmed by XRD (Fig. 10C) characterization. The presence of 200 and 220 reflections attributed to a MgO phase demonstrated that the reconstruction of LDH structure did not occur after 100 days at ambient temperature. The long-term stability of MMO films guarantees the application of the AR and AF coatings under practical conditions.

4. Conclusions

This work provides a facile and cost-effective method for the fabrication of AR and AF coatings by LBL deposition of LDH nanoparticles with PSS on quartz substrates followed by calcination. The resulting MMO films possess nanopores resulting from the removal of organic components and interlayer species of LDH nanoparticles, and thus exhibit increased transmittance and superhydrophilicity simultaneously. The influences of the size of LDH nanoparticles, the number of assembly cycle and the calcination temperature on the AR and AF properties have been studied thoroughly. A maximum transmittance of 98.7% at 650 nm and a minimum time of 0.2 s for a droplet to spread flat were achieved by calcining the $(LDH\text{-}110/PSS)_{10}$ film at 450 °C. Additionally, the present method for the fabrication of AR and AF coatings has the advantages of simplicity, easy manipulation, low-cost and large area production. The multifunctional coatings can be potentially applied in a variety of transparent materials including eyeglasses, periscopes, swimming goggles and lenses in endoscopic surgery.

Acknowledgments

This project was supported by the 973 Program (Grant No. 2011CBA00504), the National Natural Science Foundation of China and the 111 Project (Grant No. B07004).

References

[1] Y.L. Lee, D.S. Ruby, D.W. Peters, B.B. McKenzie, J.W.P. Hsu, ZnO nanostructures as efficient antireflection layers in solar cells, Nano Lett. 8 (2008) 1501–1505.
[2] S. Walheim, E. Schäffer, J. Mlynek, U. Steiner, Nanophase-separated polymer films as high-performance antireflection coatings, Science 283 (1999) 520–522.
[3] P. Yu, C.H. Chang, C.H. Chiu, C.S. Yang, J.C. Yu, H.C. Kuo, S.H. Hsu, Y.C. Chang, Efficiency enhancement of GaAs photovoltaics employing antireflective indium tin oxide nanocolumns, Adv. Mater. 21 (2009) 1618–1621.
[4] H.A. Macleod, Thin-Film Optical Filters, Elsevier, New York, 1969.
[5] J. Cho, J. Hong, K. Char, F. Caruso, Nanoporous block copolymer micelle/micelle multilayer films with dual optical properties, J. Am. Chem. Soc. 128 (2006) 9935–9942.
[6] Z. Gemici, P.I. Schwachulla, E.H. Williamson, M.F. Rubner, R.E. Cohen, Targeted functionalization of nanoparticle thin films via capillary condensation, Nano Lett. 9 (2009) 1064–1070.
[7] M.S. Park, Y. Lee, J.K. Kim, One-step preparation of antireflection film by spin-coating of polymer/solvent/nonsolvent ternary system, Chem. Mater. 17 (2005) 3944–3950.
[8] A.L. Pénard, T. Gacoin, J.P. Boilot, Functionalized sol–gel coatings for optical applications, Acc. Chem. Res. 40 (2007) 895–902.
[9] C.Y. Kuo, Y.Y. Chen, S.Y. Lu, A facile route to create surface porous polymer films via phase separation for antireflection applications, ACS Appl. Mater. Interfaces 1 (2009) 72–75.
[10] H.C. Kim, J.B. Wilds, C.R. Kreller, W. Volksen, P.J. Brock, V.Y. Lee, T. Magbitang, J.L. Hedrick, C.J. Hawker, R.D. Miller, Fabrication of multilayered nanoporous poly(methyl silsesquioxane), Adv. Mater. 14 (2002) 1637–1639.
[11] L.B. Zhang, Y. Li, J.Q. Sun, J.C. Shen, Mechanically stable antireflection and antifogging coatings fabricated by the layer-by-layer deposition process and postcalcination, Langmuir 24 (2008) 10851–10857.
[12] G.D. Fu, Z. Yuan, E.T. Kang, K.G. Neoh, D.M. Lai, A.C.H. Huan, Nanoporous ultra-low-dielectric-constant fluoropolymer films via selective UV decomposition

of poly(pentafluorostyrene)-*block*-poly(methyl methacrylate) copolymers prepared using atom transfer radical polymerization, Adv. Funct. Mater. 15 (2005) 315–322.
[13] Y. Li, F. Liu, J.Q. Sun, A facile layer-by-layer deposition process for the fabrication of highly transparent superhydrophobic coatings, Chem. Commun. (2009) 2730–2732.
[14] H. Shimomura, Z. Gemici, R.E. Cohen, M.F. Rubner, Layer-by-layer-assembled high-performance broadband antireflection coatings, ACS Appl. Mater. Interfaces 2 (2010) 813–820.
[15] L. Martinu, D. Poitras, Plasma deposition of optical films and coatings: a review, J. Vac. Sci. Technol. A 18 (2000) 2619–2645.
[16] S.L. Diedenhofen, G. Vecchi, R.E. Algra, A. Hartsuiker, O.L. Muskens, G. Immink, E.P.A.M. Bakkers, W.L. Vos, J.G. Rivas, Broad-band and omnidirectional antireflection coatings based on semiconductor nanorods, Adv. Mater. 21 (2009) 973–978.
[17] J.Q. Xi, J.K. Kim, E.F. Schubert, Silica nanorod-array films with very low refractive indices, Nano Lett. 5 (2005) 1385–1387.
[18] X. Zhang, H. Chen, H. Zhang, Layer-by-layer assembly: from conventional to unconventional methods, Chem. Commun. (2007) 1395–1405.
[19] G. Decher, Fuzzy nanoassemblies: toward layered polymeric multicomposites, Science 277 (1997) 1232–1237.
[20] D. Lee, M.F. Rubner, R.E. Cohen, All-nanoparticle thin-film coatings, Nano Lett. 6 (2006) 2305–2312.
[21] X. Liu, J. He, Superhydrophilic and antireflective properties of silica nanoparticle coatings fabricated via layer-by-layer assembly and postcalcination, J. Phys. Chem. C 113 (2009) 148–152.
[22] F. Cebeci, Z. Wu, L. Zhai, R.E. Cohen, M.F. Rubner, Nanoporosity-driven superhydrophilicity: a means to create multifunctional antifogging coatings, Langmuir 22 (2006) 2856–2862.
[23] M. Verónic, B. Graciela, A. Norma, L. Miguel, Ethanol steam reforming using Ni(II)–Al(III) layered double hydroxide as catalyst precursor kinetic study, Chem. Eng. J. 138 (2008) 602–607.
[24] J.W. Boclair, P.S. Braterman, Layered double hydroxide stability. 1. Relative stabilities of layered double hydroxides and their simple counterparts, Chem. Mater. 11 (1999) 298–302.
[25] G.R. Williams, D. O'Hare, Towards understanding, control and application of layered double hydroxide chemistry, J. Mater. Chem. 16 (2006) 3065–3074.
[26] B. Li, J. He, D.G. Evans, Experimental investigation of sheet flexibility of layered double hydroxides: one-pot morphosynthesis of inorganic intercalates, Chem. Eng. J. 144 (2008) 124–137.
[27] G. Hu, D. O'Hare, Unique layered double hydroxide morphologies using reverse microemulsion synthesis, J. Am. Chem. Soc. 127 (2005) 17808–17813.
[28] P. Benito, M. Herrero, F.M. Labajos, V. Rives, C. Royo, N. Latorre, A. Monzon, Production of carbon nanotubes from methane use of Co–Zn–Al catalysts prepared by microwave-assisted synthesis, Chem. Eng. J. 149 (2009) 455–462.
[29] L. Desigaux, M.B. Belkacem, P. Richard, J. Cellier, P. Léone, L. Cario, F. Leroux, C. Taviot-Guého, B. Pitard, Self-assembly and characterization of layered double hydroxide/DNA hybrids, Nano Lett. 6 (2006) 199–204.
[30] S. Mitchell, T. Biswick, W. Jones, G. Williams, D. O'Hare, A synchrotron radiation study of the hydrothermal synthesis of layered double hydroxides from MgO and Al_2O_3 slurries, Green Chem. 9 (2007) 373–378.
[31] E. Géraud, V. Prévot, J. Ghanbaja, F. Leroux, Macroscopically ordered hydrotalcite-type materials using self-assembled colloidal crystal template, Chem. Mater. 18 (2006) 238–240.
[32] K. Karásková, L. Obalová, K. Jirátová, F. Kovanda, Effect of promoters in Co–Mn–Al mixed oxide catalyst on N_2O decomposition, Chem. Eng. J. 160 (2010) 480–487.
[33] H. Wang, H. Yi, P. Ning, X. Tang, L. Yu, D. He, S. Zhao, Calcined hydrotalcite-like compounds as catalysts for hydrolysis carbonyl sulfide at low temperature, Chem. Eng. J. 166 (2011) 99–104.
[34] J. Han, Y. Dou, M. Wei, D.G. Evans, X. Duan, Erasable nanoporous antireflection coatings based on the "reconstruction effect" of layered double hydroxides, Angew. Chem. Int. Ed. 49 (2010) 2171–2174.
[35] Z.P. Xu, G.S. Stevenson, C.Q. Lu, G.Q. Lu, P.F. Bartlett, P.P. Gray, Stable suspension of layered double hydroxide nanoparticles in aqueous solution, J. Am. Chem. Soc. 128 (2006) 36–37.
[36] Z. Sun, L. Jin, W. Shi, M. Wei, X. Duan, Preparation of an anion dye intercalated into layered double hydroxides and its controllable luminescence properties, Chem. Eng. J. 161 (2010) 293–300.
[37] G.J. Cui, X.Y. Xu, T.J. Lin, D.G. Evans, D.Q. Li, Synthesis and UV absorption properties of 5,5′-methylenedisalicylic acid-Intercalated Zn–Al layered double hydroxides, Ind. Eng. Chem. Res. 49 (2010) 448–453.
[38] T. Chen, S. Xu, F. Zhang, D.G. Evans, X. Duan, Formation of photo- and thermo-stable layered double hydroxide films with photo-responsive wettability by intercalation of functionalized azobenzenes, Chem. Eng. Sci. 64 (2009) 4350–4357.
[39] X. Kong, S. Shi, J. Han, F. Zhu, M. Wei, X. Duan, Preparation of Glycy-L-tyrosine intercalated layered double hydroxide film and its *in vitro* release behavior, Chem. Eng. J. 157 (2010) 598–604.
[40] Z.P. Xu, G. Stevenson, C.Q. Lu, G.Q. Lu, Dispersion and size control of layered double hydroxide nanoparticles in aqueous solutions, J. Phys. Chem. B 110 (2006) 16923–16929.
[41] R. Wang, K. Hashimoto, A. Fujishima, M. Chikuni, E. Kojima, A. Kitamura, M. Shimohigoshi, T. Watanabe, Light-induced amphiphilic surfaces, Nature 388 (1997) 431–432.
[42] R. Wang, K. Hashimoto, A. Fujishima, M. Chikuni, E. Kojima, A. Kitamura, M. Shimohigoshi, T. Watanabe, Photogeneration of highly amphiphilic TiO_2 surfaces, Adv. Mater. 10 (1998) 135–138.
[43] M. Miyauchi, A. Nakajima, K. Hashimoto, T. Watanabe, A highly hydrophilic thin film under 1 $\mu W/cm^2$ UV illumination, Adv. Mater. 12 (2000) 1923–1927.